Title: Calcium activation of frequency dependent temporally phasic, localized, and dense population of cortical neurons by continuous electrical stimulation

Nicholas J. Michelson[1], Riazul Islam[1,2], Alberto L. Vazquez[1,2,3,4,5], Kip A Ludwig[6], Takashi DY Kozai[1,2,5,7,8]

1. Department of Bioengineering, University of Pittsburgh
2. Center for the Neural Basis of Cognition, University of Pittsburgh
3. Department of Radiology, University of Pittsburgh
4. Department of Neurobiology, University of Pittsburgh
5. Center for Neuroscience, University of Pittsburgh
6. Department of Biomedical Engineering, University of Wisconsin Madison,
7. McGowan Institute of Regenerative Medicine, University of Pittsburgh
8. NeuroTech Center, University of Pittsburgh Brain Institute

*Correspondence: tdk18@pitt.edu

Abstract

Electrical stimulation of the brain has become a mainstay of fundamental neuroscience research and an increasingly prevalent clinical therapy. Despite decades of use in basic neuroscience research over acute time scales, and the growing prevalence of neuromodulation therapies, gaps in knowledge regarding activation or inactivation of neural elements over time in the vicinity of the electrode limit the ability to adequately interpret evoked downstream responses or fine-tune stimulation parameters to focus on the desired response. In this work, *in vivo* two-photon microscopy was used to image Thy1-GCaMP activity in Layer 2/3 neurons of S1 cortex during 30 s of continuous electrical stimulation at varying frequencies. We show that during continuous stimulation, stimulation frequency influences a distinct spatial and temporal pattern of somatic activation. Our results elucidate conflicting results from prior studies reporting either dense spherical activation of somas biased towards somas near the electrode, or sparse activation of somas at a distance via axons near the electrode. These findings indicate that the neural element specific temporal response local to the stimulating electrode as a function of changes in charge density applied, frequency and temporal patterning need to be considered to properly interpret downstream circuit responses for basic science understanding, or determining mechanisms of action for clinical therapeutic applications.

Keywords : microstimulation, bioelectric medicine, brain-computer interface, deep brain stimulation, neuroprosthetics

Introduction

Understanding complex nervous systems requires the ability to readout detailed measurements from controlled inputs[1-4]. While many new techniques and technologies are emerging, electrical stimulation remains one of the oldest and most widely used methods for directly interfacing and driving the nervous system[5-9]. The ability to directly apply electrical potentials to individual nerves has helped identify biophysical properties of nerves and neurons[10,11], and has been crucial in understanding the organization of the brain[12,13]. These studies also opened the door for applying electrical stimulation for therapeutic applications[14]. Electrical stimulation has been used for hearing[15-18], vision[19,20], and somatosensory restoration[21,22], and to treat movement disorders[23-26], chronic pain[27-30], and epilepsy[31,32]. More recently there has been an expansion of neuromodulation clinical trials, with over 1000 clinical trials registered on clinicaltrials.gov utilizing implanted or non-invasive electrodes to activate/inactivate nervous tissue to treat diverse conditions such as Tourette's syndrome, obsessive compulsive disorder, depression, Alzheimer's disease, and stroke. These clinical applications further motivate the development of improved chronically implanted electrical stimulation devices[33].

Despite its growing prevalence in scientific and clinical research, there is limited understanding of how electrical stimulation directly interacts with the complex milieu of neuronal and non-neuronal cells in the brain near the electrode. In acute mapping experiments of peripheral nerve fibers, short pulses of electrical stimulation were hypothesized to activate a small sphere of fibers in the local vicinity of the electrode[34-37], with increases in amplitude increasing the volume of the sphere activated. When applying cathodic leading stimulation waveforms, increasing the amplitude could also cause a small zone of inactivation near the electrode tip, due to the generation of virtual anodes more distant from the tip hyperpolarizing axons, ultimately preventing the propagation of any action potentials[35]. In contrast, recent experiments utilizing 2-photon calcium imaging to visualize the activation of neural elements in cortex near the electrode site found that electrical stimulation activated a sparse population of neuronal somas distant from the electrode site[38]. These experiments demonstrated that electrical stimulation activates a much smaller volume of neural processes around the electrode tip, which in turn activate the connected soma[38].

Although changes in pulse amplitude are widely understood to alter the area of activation within the vicinity of the electrode, the extent to which different stimulation frequencies and pulse train durations affect local neuronal responses remain less explored. In this study, *in vivo* multiphoton calcium imaging was employed GCaMP6 mice to elucidate how neuronal elements near an implanted electrode respond to different electrical stimulation frequencies over the course of a longer pulse train. Transgenic GCaMP6 mice allow for the probing of neuronal activity with high SNR/fidelity in a large proportion of cortical excitatory neurons without the need for exogenous calcium chelators. Stimulation was carried out at different frequencies using a 30 second burst of cathodic leading symmetric pulses, with a 50 μs pulse width/phase and pulse amplitudes within the established Shannon safety limits to avoid tissue damage (Shannon criteria of k between 0.12 and 1.3, 2.5 nC per phase). We demonstrate that different neural elements (neurites, soma) in the vicinity of the electrode differ in their responses as a function of time (stimulation onset, during, and after stimulation), space, and stimulation frequency. These data show a complex response profile of nervous tissue near the electrode to electrical stimulation that may have significant implications for the design of electrical neuromodulation experiments and therapies.

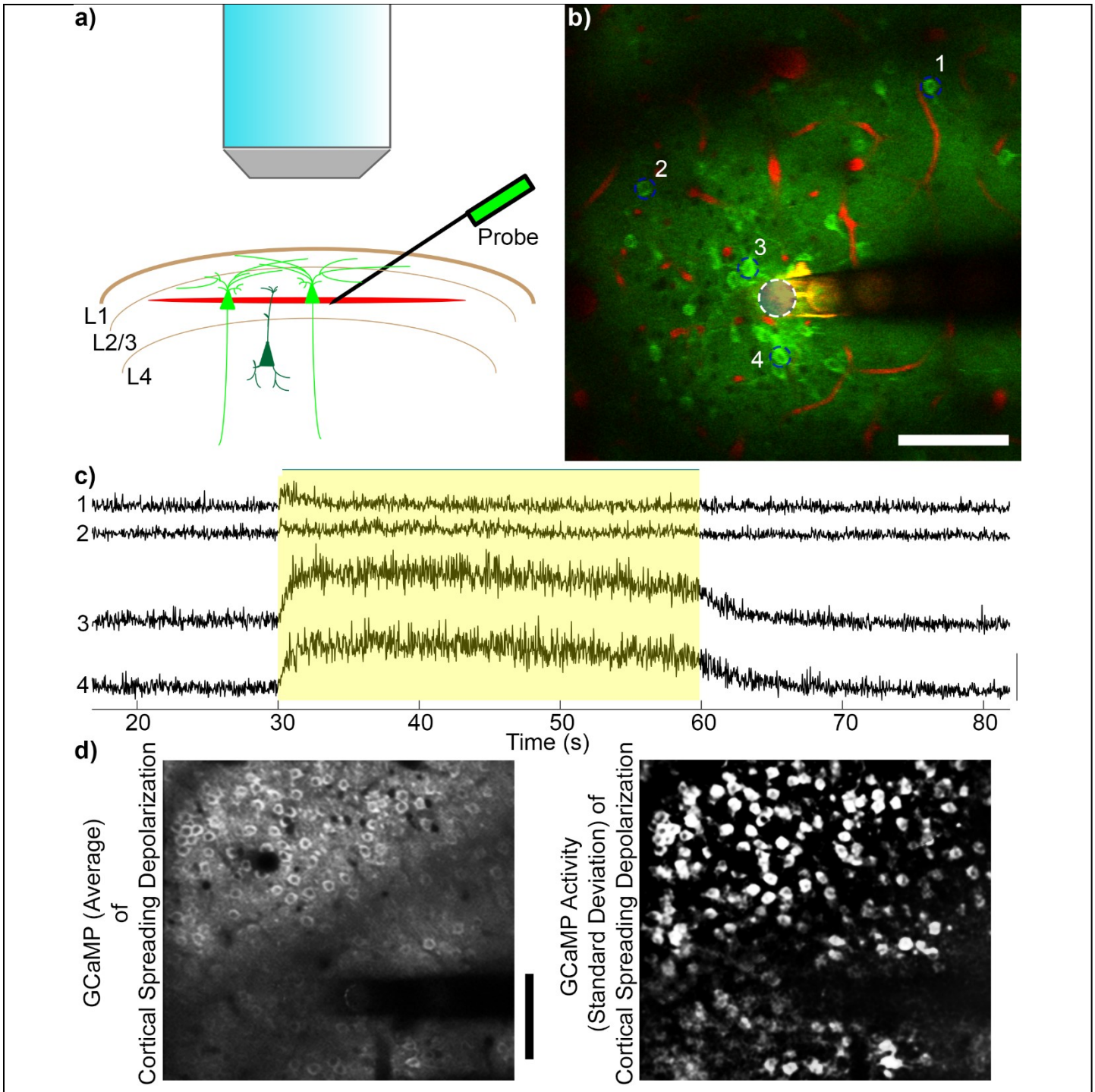

Figure 1: Experimental setup for imaging continuous stimulation evoked calcium activity. a) Microelectrodes were implanted into Layer II/III of S1 Cortex. Red region indicates the imaging plane. b) 1 s average of GCaMP6 activation around the implanted microelectrode during 90 Hz stimulation. White dashed circle indicates the activated electrode site. GCaMP intensity of numbered cells indicated by dashed blue circles are shown in (c). Yellow indicates duration of stimulation (30 s). Scale indicates detected intensity of 500. D) Average (left) and standard deviation (right) of GCaMP activity during a cortical spreading depression shows dense labeling of neurons. Scale bar = 100 µm.

Results

In vivo two-photon calcium imaging of ketamine-anesthetized GCaMP6 transgenic mice was used to study the spatiotemporal activation pattern of neurons during microstimulation. Neurons in layer II/III of S1 somatosensory cortex were imaged as previously described[39], and electrically stimulated continuously for 30 s at different frequencies (Fig 1a). GCaMPs are genetically encoded intracellular calcium indicators that largely reflect action potential firing[40-45]. Because quiescent neurons have low GCaMP fluorescence, capillary visualization using 0.1 mg of sulforhodamin101 (SR101) was used to ensure the location of the electrode and

visibility in the tissue with low laser power (< 20 mW), as previously described (Fig 1b)[39,46-51]. Although GCaMP6 is more sensitive compared to other calcium indicators, such as Oregon green BAPTA, it has a longer decay constant that did not impair detection of activity[45]. Evoked fluorescence traces show considerable variability in the intracellular calcium response to continuous stimulation (Fig 1c). The mouse line used in this study (GP4.3Dkim/J) has relatively high expression levels of GCaMP in layer II/III neurons[40], which was corroborated in a separate study, where this mouse line was imaged during a cortical spreading depression (Fig. 1d). The results demonstrate that sparse GCaMP activation noted during electrical stimulation is not due to sparse GCaMP expression in the genetic line.

The laminar probes were inserted with the electrode sites facing up and the imaging plane positioned approximately 10-15 μm above the electrode site in order to capture the neurons just above the stimulation site. The position of the imaging plane was confirmed through anatomical Z-stacks taken prior to the experiment. Co-registration of vasculature features, outline of the implanted probe, and the electrode sites and traces were used to ensure that imaging plane was just above the electrode site throughout the experiment. Electrical stimulation parameters matched previously employed protocols for neuroprosthetics and neuromodulation applications[52-56]. Stimulation pulses were cathodic leading biphasic symmetric waveforms with pulse widths of 50 μs/phase[57]. Stimulation was performed for 30 s at a charge density below the Shannon safety limit for planar iridium electrode sites with 703 μm^2 surface area[58]. In general, stimulation was delivered at 50 μA and 50 μs, which has been previously been shown to be just above the sensitivity threshold[55]. The stimulation frequency was varied over different trials (Fig. 2; 10, 30, 50, 75, 90, 130, 250 Hz). As expected from previous reports[38], electrical stimulation led to sparse, distributed activation patterns (Fig. 2) Frequencies of 50 Hz and 130 Hz were selected as they are the frequencies at which the Shannon/McCreery safety curve was developed and the average optimal therapeutic frequency for DBS in Parkinson's Disease patients, respectively[58,59].

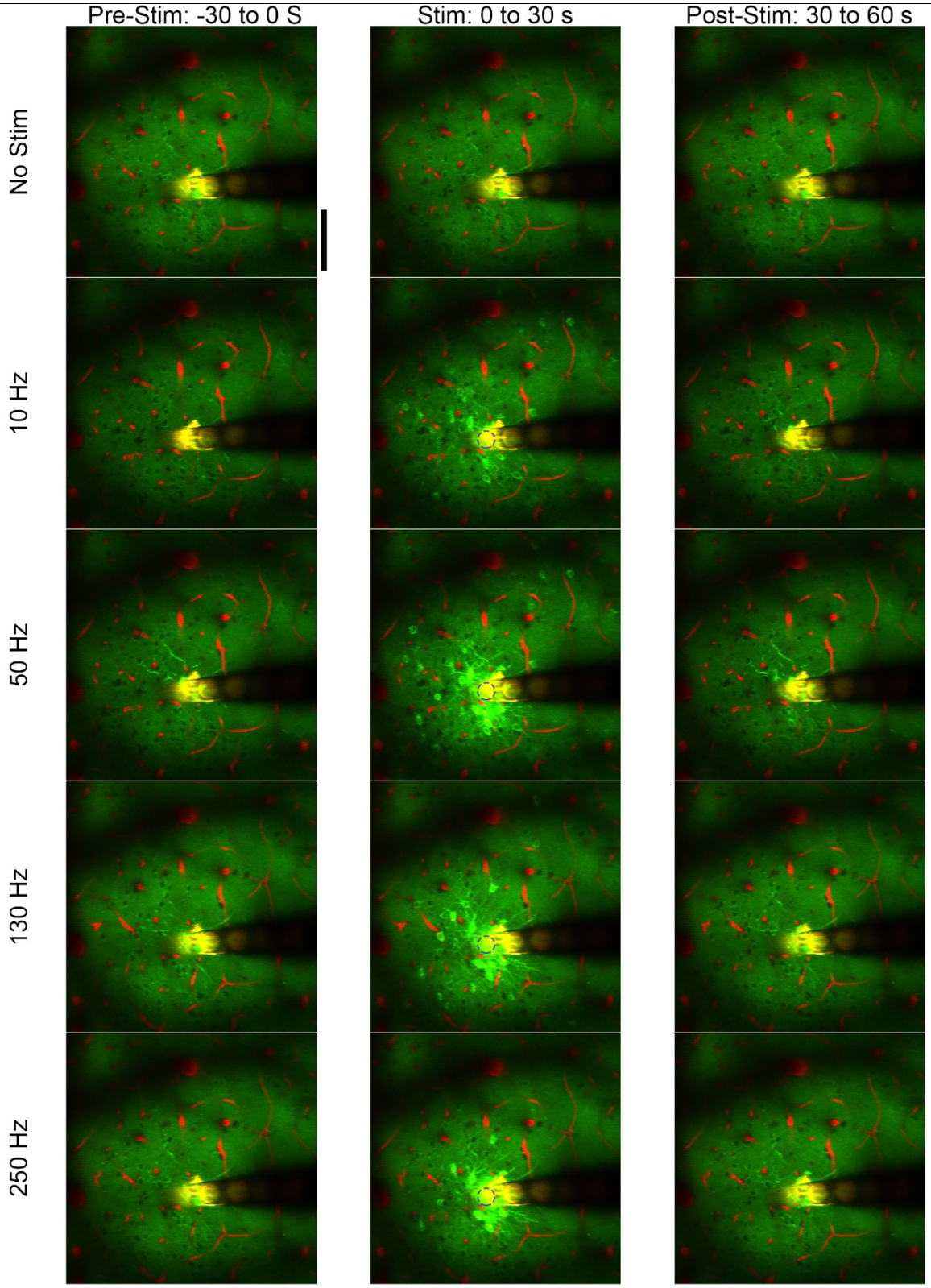

Figure 2: Stimulation frequency influences GCaMP activation pattern. Mean GCaMP imaging of 30 s prior to stimulation (left), during stimulation (middle), and post-stimulation (right) at no stimulation, 10 Hz, 50 Hz, 130 Hz, and 250 Hz. Green indicates GCaMP labelled neurons and red indicates vasculature. The electrode sites and traces reflect fluorescence in both channels and therefore appear in yellow. Different patterns of activation can be observed at different frequencies, and GCaMP activity returns to baseline by 30 s post-stimulus. Scale = 100 µm. *k*=-0.12.

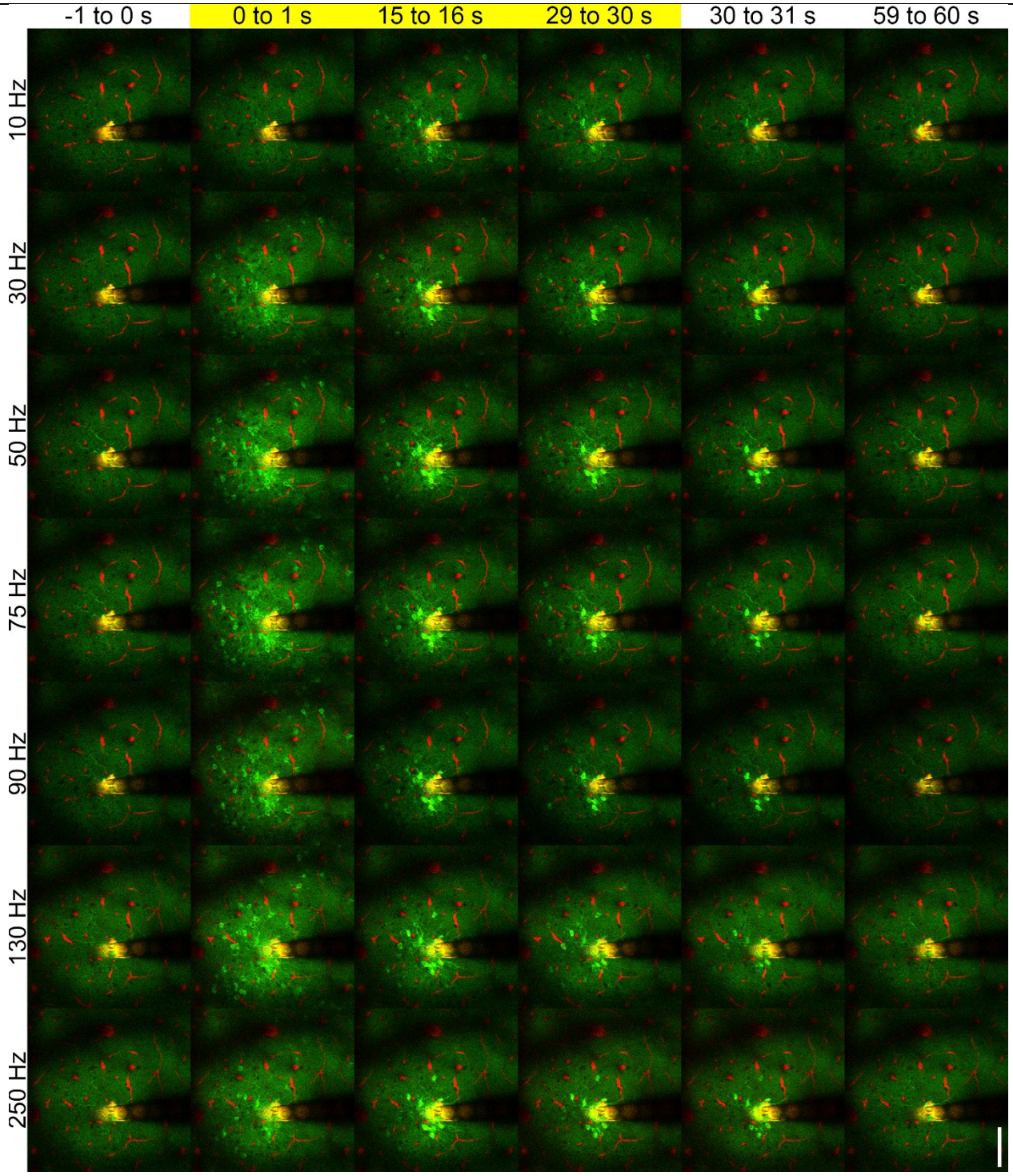

Figure 3: Continuous electrical stimulation evokes frequency dependent temporal activation. Mean GCaMP activity immediately before stimulation (-1 to 0s), at stimulation onset (0 to 1s), during stimulation (15 to 16s), immediately before stimulation termination (29 to 30s), immediately after termination (30 to 31s) and after stimulation (59 to 60 s). While the activation of GCaMP is lower at 10 Hz, GCaMP activation pattern is similar at onset across frequencies. However, the activation pattern at the end of the stimulation train (29 to 30 s) differs based on frequency of the stimulation. Images taken from the same animal and trials as figure 2. Scale = 100 μm. *k*=-0.12.

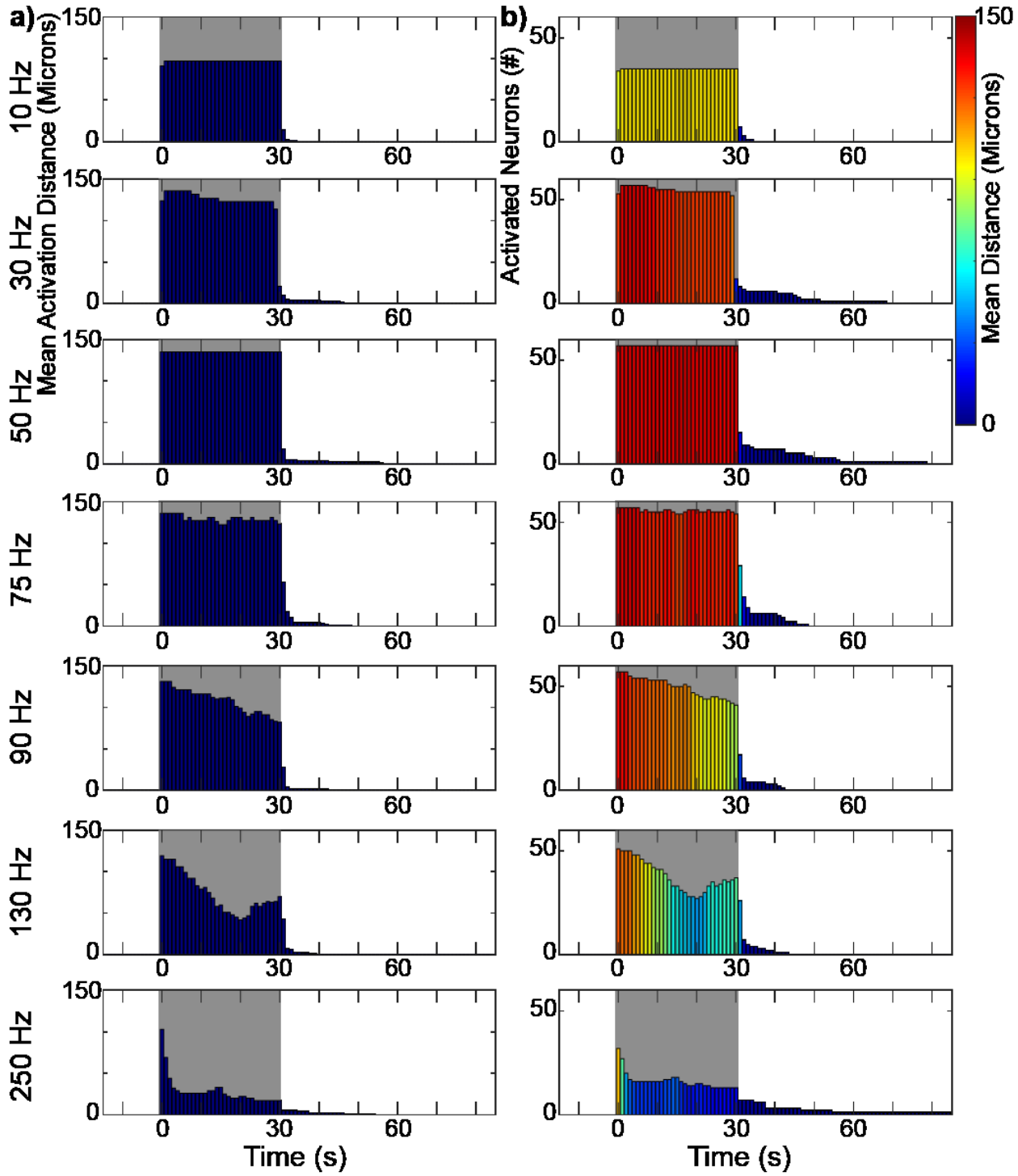

Figure 4: Spatial and temporal distribution of frequency dependent GCaMP activation in a representative animal. a) The average number of active neurons during electrical stimulation (grey box) decreases over time at higher frequencies. The mean activation distance shows that electrical stimulation at higher frequencies (>90 Hz) leads to a decrease in the average distance of calcium activity over long stimulation pulse trains (color).

Continuous stimulation elicits two populations of neural activation with distinct spatiotemporal responses

Changes in intensity of neuronal activation over the course of the 30 s pulse train were evident, with dramatically different temporal responses between local and distant neurons. In general during the onset, a pulse train activated both local and distant neurons (Fig. 3, 4). However, for frequencies > 10 Hz, as the pulse trained continued, distant neurons would cease to be activated, resulting in a marked difference in distal neural activation at the end of a pulse train. This effect became more pronounced as frequency was increased. As can be seen in Figure 4b, at lower frequencies (10-75 Hz), the number of neurons activated across time during the pulse train is relatively constant. At frequencies at 90 Hz or greater, there is a clear fall off in the number of

neurons activated as the pulse train progresses, with duration of Activation Time for distant neurons becoming shorter as frequencies are increased from 90 to 250 Hz, with a very sharp fall-off in number of active neurons at 250 Hz on the order of 5 seconds (Figure 4 and b).

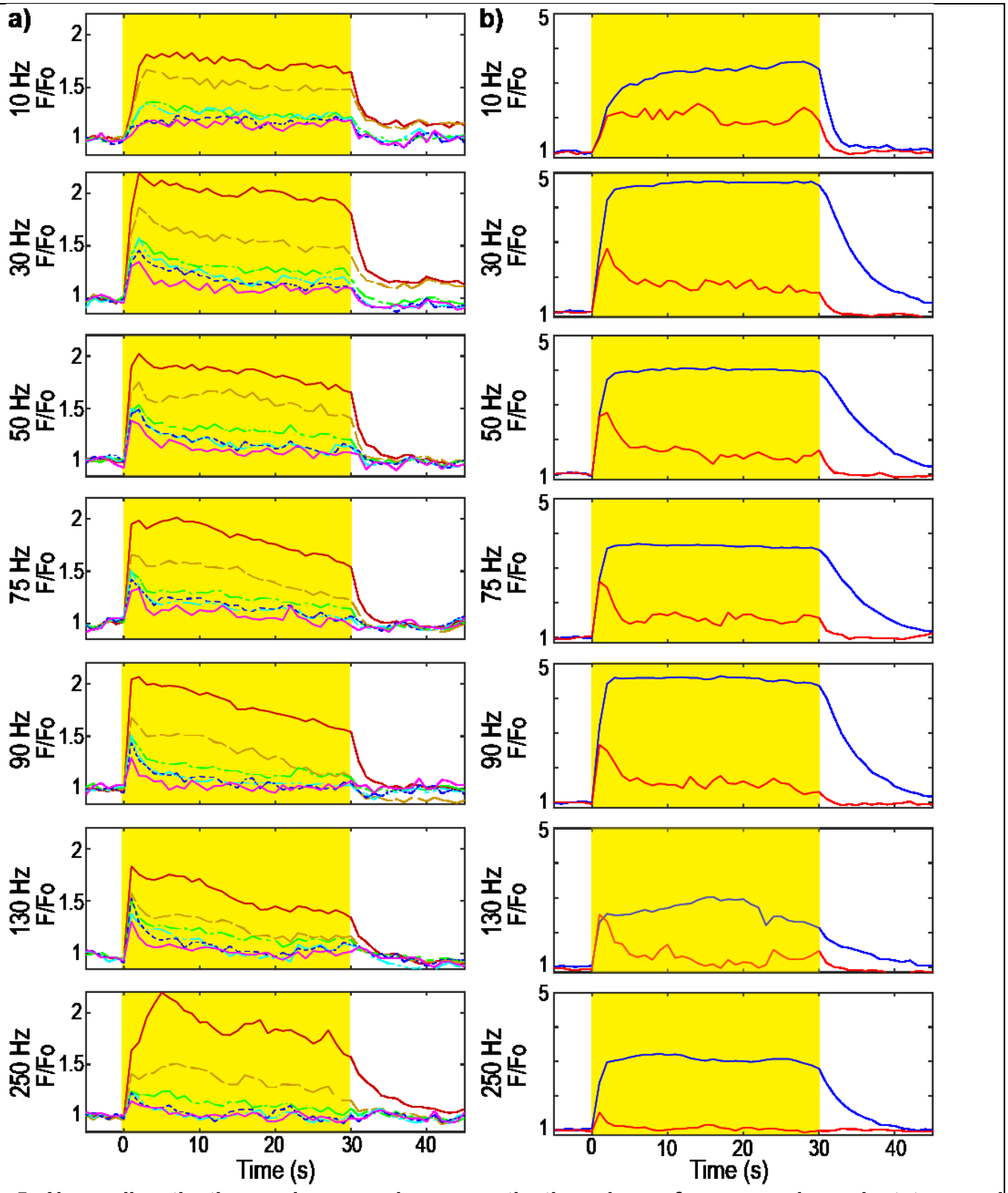

Figure 5: Neuropil activation and neuronal soma activation shows frequency dependent temporal falloff. a) GCaMP neuropil activation at 10-20 µm (red, solid line), 30-40 µm (orange, dashed line), 50-60 µm (green, -·-), 100-110 µm (cyan, -···-), 150-160 µm (blue, dotted line), and 245-255 µm (violet, solid line). Spatial and temporal neuropil falloff increase with frequency. **b)** GCaMP activation in the soma at 15 µm (blue) or 115 µm (red). Yellow indicates the stimulation. F_0 is the mean intensity of the pre-stimulus period.

Neuropil GCaMP Activity

An analysis of neuropil activation as a function of distance from the electrode, time post-stimulation onset, and frequency of stimulation was also performed (Fig. 5). Since the neuropil is composed of neurites from surrounding cells, it is understood to represent a spatial average of nearby responding and non-responding cells[38]. In this analysis, regions of interest previously identified as isolated somas were removed, and the average changes in GCaMP intensity in the remaining volume were assessed. Across all frequencies tested, there is a more linear fall off in stimulation evoked GCaMP intensity as a function of distance from the electrode as opposed to the fall off observed for the number of activated somas. In contrast to the neuropil, example neurons near (15 μm) the electrode site show gradual increase in GCaMP intensity at 10 Hz and a rapid plateau between 30 to 90 Hz (Fig. 5b, blue; 15 μm). However, similar to the time course of distant soma activation (Fig. 5b, red; 115 μm), there is a peak in activation of the neuropil in the first five seconds post stimulation, with a decrease in activation thereafter. At 10 Hz the decrease in neuropil activation is slower across all distances, with the peak and subsequent decay more steep (slope of F/Fo) for higher frequencies. There is also a post-stimulus residual activation for both the neuropil and local neurons (Fig. 5a b). This residual increase in activation can last up to 30 seconds or more post stimulation (Fig. 4b) for somas, but is typically shorter in duration for the neuropil (Fig. 5a). This may partially be a function of GCaMP saturation in different elements of the neuron leading to different decay kinetics, but the duration of the somatic residual response is notably longer than can be solely accounted for by the decay in intensity of the GCaMP fluorophore after maximal activation[45].

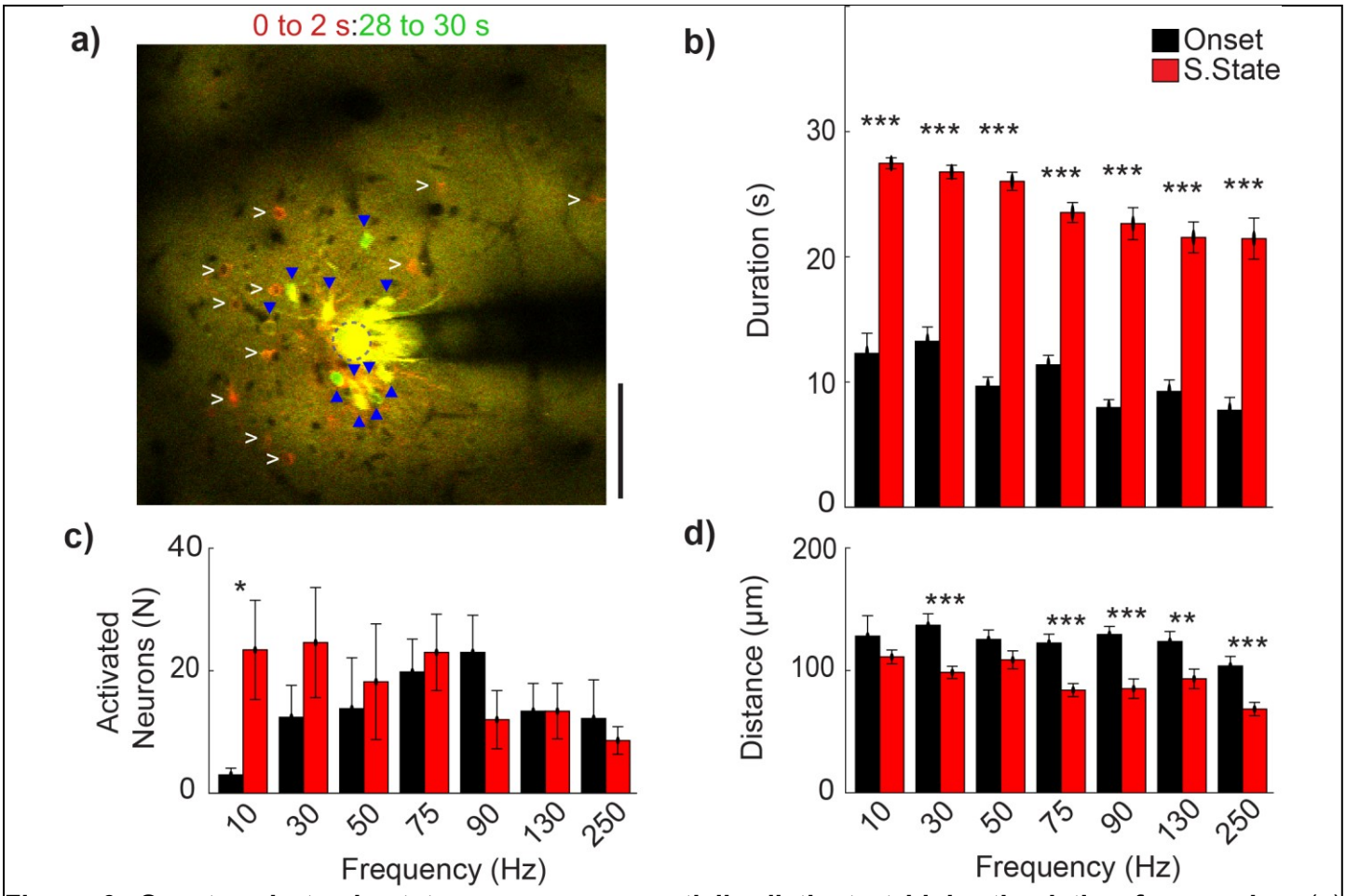

Figure 6: Onset and steady-state neurons are spatially distinct at high stimulation frequencies. (a) Mean GCaMP activity at the onset of the stimulation (0 to 2 s; red) and immediately before the end of stimulation (28 to 30 s; green) (stimulation parameter: 250 Hz, 50µA). Onset neurons (white arrowheads) and steady-state: (blue triangle) are marked in both images. It should be noted that, several steady-state neurons were active even at the onset of stimulation (yellow). (c) Average duration of onset and steady-state phase. Duration of activation phases were calculated by tracking onset-responsive (neurons that are active 0-2s into stimulation) and steady-state-responsive neurons (neurons active 28-30s into stimulation). (b) Average number of neurons activated during onset and steady-state phase for 10Hz, 30Hz, 50Hz, 75Hz, 90Hz, 130Hz and 250 Hz stimulation. (d) Average distance of the neurons activated during onset and steady-state phase. With increasing frequency, onset activated neurons are located significantly further from the electrode site than steady-state neurons. *P < 0.05, **P < 0.01 and ***P < 0.001, two sample t-test. Data are mean ± SEM (n = 5).

Stimulation in somatosensory cortex activates neurons with different temporal activation behavior

Continuous electrical stimulation led to a frequency dependent temporal pattern of activation which was separated into 1) onset neurons that rapidly decline in activity and 2) steady-state neurons that remain activated throughout the stimulation period. Since different spatiotemporal activation patterns were observed during the stimulation period in an individual mice (Fig. 3), the aggregate temporal properties of onset and steady-state neurons were examined and summarized for all mice (n=5). To differentiate between these groups, somas that were still activated during the last two seconds of the stimulation period were defined as steady-state neurons. Neurons that were activated during the first two seconds of the stimulation period, but not during the final 2 seconds of the pulse train were defined as onset neurons (Fig. 6a). The duration of onset and steady-state neuron activity was measure by quantifying the total time during the stimulation period that GCaMP intensity was greater than an intensity threshold of three-standard deviations from the average of the pre-stimulus period. Steady-state neurons had a significantly greater duration of activity than onset neurons(10 Hz: 27.5±0.4 s, 30 Hz: 26.8±0.5 s, 50 Hz: 26.0±0.7 s, 75 Hz: 23.5±0.8 s, 90 Hz: 22.6±1.3 s, 130 Hz: 21.6±1.2 s, 250 Hz: 22.5±1.6 s; compared to the duration of onset activated neurons at 10 Hz: 12.3±1.6 s, 30 Hz: 13.3±1.1 s, 50 Hz: 9.7±0.7 s, 75 Hz: 11.4±0.8 s, 90 Hz: 8.0±0.6 s, 130 Hz: 9.2±0.9 s, 250 Hz: 7.8±1.0 s) (Fig.

6c, p < 0.001, two sample t-test). There were significantly less onset neurons for 10 Hz stimulation compared to steady-state neurons, indicating most of the somas were steady-state neurons (Fig. 6c, $p<0.05$).

In order to evaluate if there was a spatial relationship to onset and steady-state somas, the spatial distribution of the two populations were compared (Fig. 5a). Since charge density accumulates on the edges of planar electrode sites,[60] distances were measured from the center of each soma to the nearest edge of the stimulating electrode site. Steady-state neurons were generally located closer to the electrode site than onset neurons, on average by ~40 µm (Fig. 6d, 30 Hz: 98.4±5.0 vs. 136.9±9.3 µm, respectively, 75 Hz: 83.9±5.3 vs. 122.4±7.2 µm, 90 Hz: 85.1±7.9 vs 129.3±6.6 µm, 130 Hz: 93.1±8.0 vs. 123.6±8.1 µm, 250 Hz: 68.4±5.5 vs 103.6±7.7 µm). Neurons separated as onset neurons and steady-state neurons show distinct spatial relationships that are distant or proximal to the stimulation electrode, respectively.

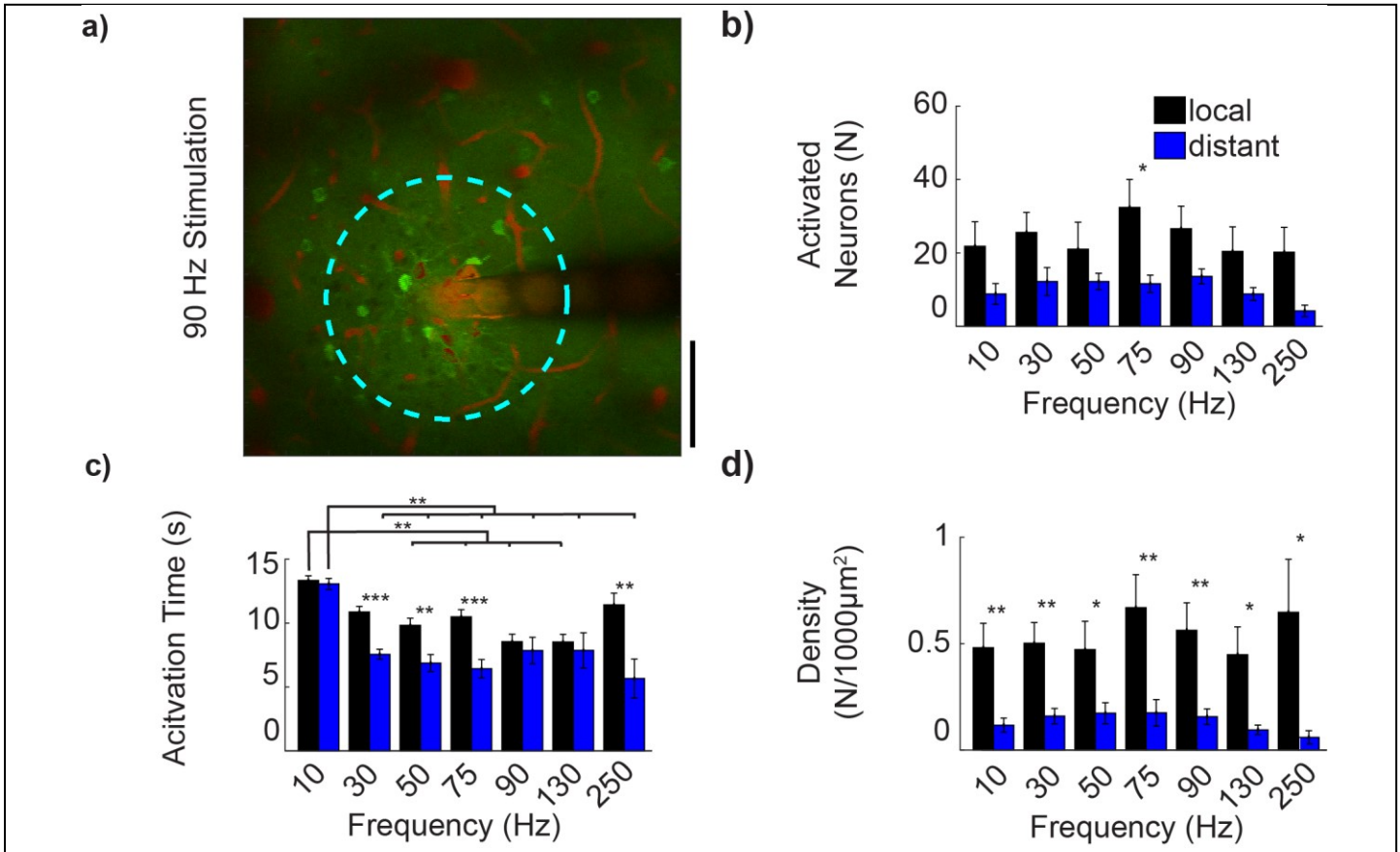

Figure 7: Activation properties of local and distant neuronal populations. (a) Standard deviation intensity projection over 30 seconds following 90Hz stimulation. Distance threshold shown by cyan circle. (b) Average number of neurons activated that are local and distal from the electrode. (c) Average activation time for local and distant activated neuron populations. (d) Average activation density of local and distal neuron population. Activation density for locally activated neurons was significantly higher for all stimulation frequencies than distally activated neurons. *P < 0.05, **P < 0.01 and ***P < 0.001, two sample t-test and one-way analysis of variance (ANOVA) with Bonferroni post hoc analysis. Data are mean ± SEM (n = 5).

Stimulation in somatosensory cortex activates local and distant neurons in a frequency dependent manner

During continuous electrical stimulation distant somas decrease in activity at higher frequencies (Fig. 6d). However, Figure 6a shows variability in the distance threshold for onset and steady-state neurons. While stimulation at frequencies greater than 10 Hz led to onset and steady-state neurons exhibiting a significant spatial relationship, not all onset neurons were distant neurons, and not all distant neurons were steady-state neurons. Therefore, in order to minimize methodological bias, somas were also grouped by distance to evaluate if 'local' and 'distant' neurons exhibited distinct temporal relationships. Somas were classified as local and distant cells by establishing a distance threshold (see methods, Fig. 7a,b), which was calculated in each trial from the distribution of distances from each activated soma (10 Hz 165.9±26.7 µm; 30 Hz 163.8±19.2 µm;

50 Hz 187.8±17.0 μm; 75 Hz 197.1±20.0 μm; 90 Hz 197.9±24.0 μm; 130 Hz 197.9±24.0 μm; 250 Hz 165.1±21.7 μm).

To evaluate if local and distant somas had different temporal activation patterns, the Activation Time of the two populations were compared. Somatic calcium changes generally reflect action potential firing; although during periods of high spike rates, GCaMP6 fluorescence intensity can saturate due to the long decay constant[45]. Because distant somas may exhibit a stimulation evoked burst of activity, which can be followed by a period of lower activity throughout the rest of the stimulation period (Fig. 5b; red), stimulation duration did not effectively capture the bursting dynamics of these neurons. Therefore, to evaluate if local and distant somas had different temporal activation patterns, the 'Activation Time' of the two populations were compared. The Activation Time was defined as an estimate of the mean time at which the cell is responsive, weighted by the GCaMP intensity, and was calculated as the time-point at which the cumulative intensity reached 50% of the maximum cumulative ΔF/F signal change during the stimulation period. Activation Time was significantly greater in local somas than in distant somas for 30 Hz (10.9±0.4 vs 7.6±0.4 s), 50 Hz (9.8±0.6 vs 6.9±0.7 s), 75 Hz (10.5±0.6 vs 6.4±0.7 s), and 250 Hz (11.4±0.9 vs 5.7±1.5 s) stimulation (Fig. 7c, $p<0.05$). Additionally, Activation Time of both local and distant somas showed significant frequency dependence (Fig. 7c, $p<0.05$). Particularly of note was that for 10Hz stimulation, the local somas had significantly greater Activation Time than higher stimulation frequencies ($p<0.01$).

As a spatial pattern of activation was observed during continuous stimulation (Fig 7c), the activation density for local and distant populations was measured. Activation density for local somas was calculated as the number of somas activated within the distance threshold, divided by the total area encompassed by the threshold. For distant somas, activation density was calculated using the area encompassed by an annulus with inner radius, *r*, equal to the distance threshold, and outer radius, *R*, equal to the distance of the furthest soma. For all stimulation frequencies, local neurons had significantly greater neuronal density than distant somas (Fig. 6d, $p<0.05$; 10 Hz 0.525±0.097 vs 0.116±0.027 N/1000μm^2; 30 Hz 0.567±0.085 vs 0.174±0.026 N/1000μm^2; 50 Hz 0.523±0.126 vs 0.168±0.042 N/1000μm^2; 75 Hz 0.717±0.129 vs 0.171±0.52 N/1000μm^2; 90 Hz 0.605±0.102 vs 0.161±0.033 N/1000μm^2; 130 Hz 0.475±0.116 vs 0.997±0.019 N/1000μm^2; 250 Hz 0.667±0.244 vs0.0593±0.029 N/1000μm^2, respectively). Local activated somas had longer Activation Times and greater densities than distant somas.

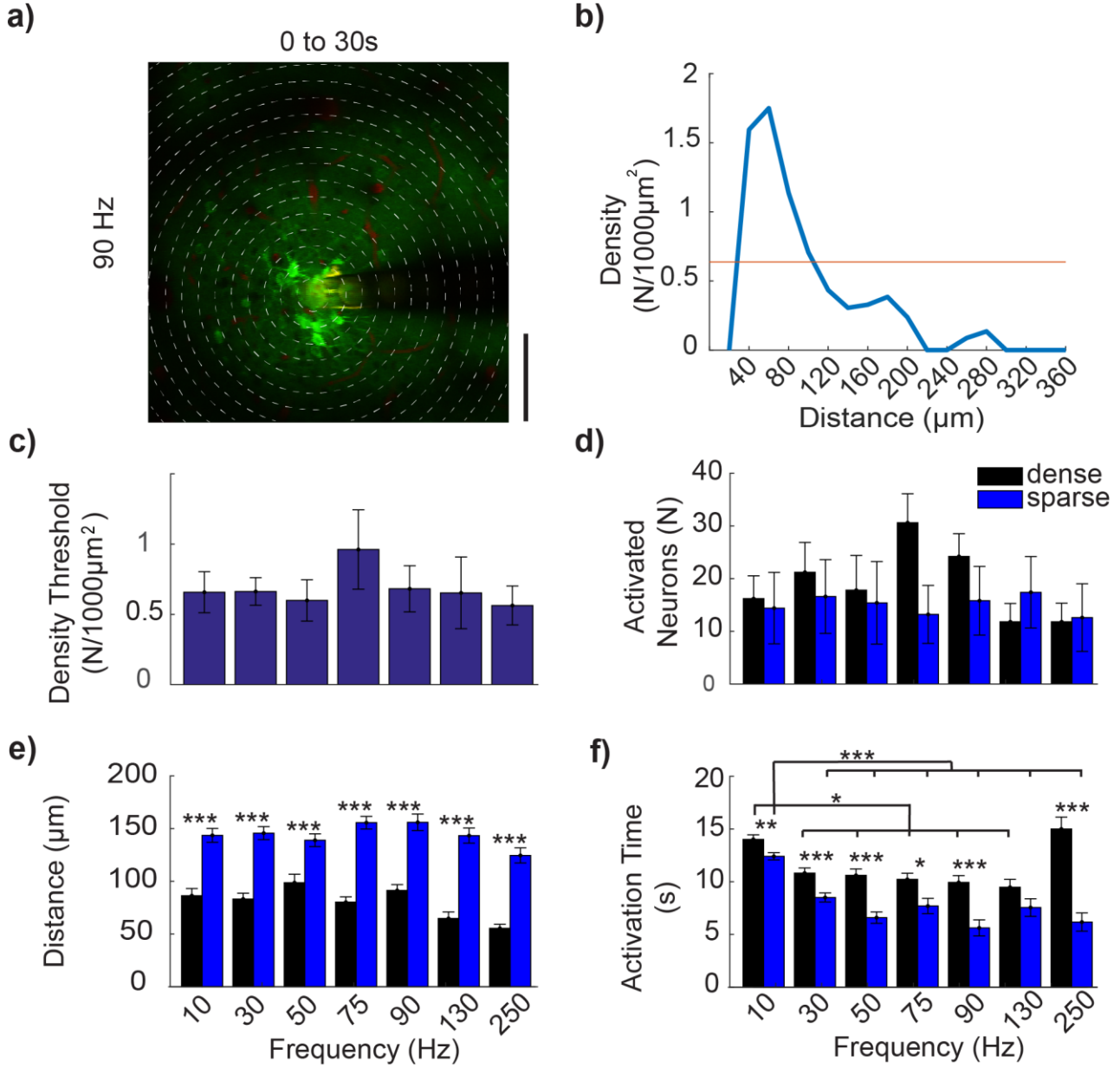

Figure 8: Activation properties of dense and sparse populations of neurons. (a) Mean GCaMP activity (30 s, 90 Hz stimulation) with concentric bins of 20 μm incremental radius around the center of the electrode site, demonstrating density calculation method. (b) For the same trial, density (N/1000 μm^2) is plotted against distance of the bins from the electrode. (c) Average density threshold of 10Hz, 30Hz, 50Hz, 75Hz, 90Hz, 130Hz and 250 Hz stimulation. Density threshold was calculated from mean density + 1SD for the entire 30s stimulation. Threshold density value separates dense and sparse activated neurons. (d) Number of activated neurons in dense and sparse populations. (e) Average distance of dense and sparse activated neurons. For all stimulation frequencies, sparsely activated neurons are located further from the electrode site than dense activated neurons. (f) Average activation time of dense and sparse activated neuron population. Dense activated neurons are active for a longer duration in all stimulation frequency except 130Hz. *P < 0.05, **P < 0.01 and ***P < 0.001, two sample t-test. Data are mean ± SEM (n = 5).

Stimulation in somatosensory cortex creates a frequency dependent activation density pattern

Prolonged electrical stimulation led to a dense activation pattern due to a decrease in activity in distant somas at frequencies >10 Hz. Similarly as before, in order to address potential biases that may arise from the employed computational categorization methods of time and distance, somas were separated into dense and sparse populations using a density threshold and evaluated for distinct spatial and temporal relationships. In order to evaluate if continuous electrical stimulation can activate a set of cells restricted to a small spatial volume, patterns of somatic activation were classified as dense or sparse. Concentric circular bins were drawn

with their origin at the center of the electrode site with subsequent bins increasing in 20 μm radial increments (Fig. 8a). Density was calculated as the number of activated neurons in each bin, divided by the concentric bin area (Fig 8b). Density thresholds were established similarly to distance thresholds (10 Hz 0.657±0.146 N/1000μm^2; 30 Hz 0.663±0.098 N/1000μm^2; 50 Hz 0.599±0.147 N/1000μm^2; 75 Hz 0.963±0.282 N/1000μm^2; 90 Hz 0.682±0.164 N/1000μm^2; 130 Hz 0.653±0.255 N/1000μm^2; 250 Hz 0.563±0.139 N/1000μm^2 (Fig. 8c-d).

Activated somas within dense populations were located significantly closer to the electrode site for all stimulation frequencies (Fig. 8e, $p<0.001$; 10 Hz 86.4±6.9 vs 143.6±6.6 μm; 30 Hz 83.2±5.5 vs 145.7±6.1 μm; 50 Hz 98.7±8.0 vs 138.9±6.0 μm; 75 Hz 80.2±5.1 vs 155.6±6.0 μm; 90 Hz 90.3±5.6 vs 156.0±7.8 μm; 130 Hz 60.7±6.2 vs 143.3±7.2 μm; 250 Hz 55.4±3.9 vs 124.5±7.1 μm, respectively). The distance of densely activated somas was largest during 50 Hz stimulation (Fig. 8e, $p<0.05$ for 50 vs 130 Hz and $p<0.001$ for 50 vs 250 Hz). Additionally, densely activated somas demonstrated significantly greater Activation Times compared to sparsely activated somas (Fig. 8f, $p < 0.05$ for 10 Hz (14.0±0.3 vs 12.4±0.4 s, respectively), 30 Hz (10.8±0.4 vs 8.5±0.5 s), 50 Hz (10.6±0.5 vs 6.6±0.6 s), 75 Hz (10.2±0.7 vs 7.7±0.6 s), 90 Hz (9.9±0.8 vs 5.6±0.7 s), and 250 Hz (15.0±0.9 vs 6.2±1.1 s)). The Activation Time of dense and sparse somas showed similar frequency dependence as observed in local and distal somas in Fig. 7c. Stimulation activated somas that were classified as higher density were closer to the electrode and had longer Activation Time compared to low density classified regions, which were further from the electrode and had shorter Activation Times. At the onset of electrical stimulation, there is a low density, sparse, and distributed activation pattern of neurons. However, Figures 2-8 taken together show that during prolonged continuous electrical stimulation, the activated somas showed a strong relationship between longer Activation Times, closer proximity to the electrode, and higher activation density at frequencies >10 Hz.

Discussion:

Previous work by Histed et al utilizing 2-photon microscopy and a calcium indicator demonstrated that stimulation with <1 s pulse trains of cathodic phase leading, 200 μs/phase, biphasic pulses under 10 μA in current at 250 Hz, results in a sparse, distributed population of neurons activated surrounding the electrode tip, without a strong bias towards activation of neurons near the tip[38]. Increasing current over the 4-9 μA range increased the density of neurons activated within this 100-200 μm sphere, again without a bias towards more neurons activated closer to the tip[38]. Through multiple experimental manipulations they concluded that stimulation in this confined parameter range only directly activates axons within 30 μm of the electrode, which in turn antidromically activates the somas associated with these axons, yielding the observed sparse pattern of somatic activation[38]. These results were counter to prevailing theory based on seminal studies by Stoney et al suggesting that stimulation leads to a sphere of activated neurons near the electrode tip, with the size of the sphere growing in proportion to the current applied[34-37,61-63].

The Histed results were obtained using stimulation charges at or just above the threshold for eliciting a significant response using a calcium indicator (0.8 to 1.8 nC/phase), applied for brief periods (<1 s) and at very high frequency (250 Hz), which led to the implication that, “it is impossible to activate a set of cells restricted to a small spatial volume”[38]. In contrast, the results described in our present study were obtained using longer pulse trains (30 s) at comparatively large stimulation charges (2.5 nC/phase) to better match limits established for sensory perception in behaving experiments[55]. Utilizing these parameters, across frequencies we observed a distinct pattern of somatic activation consisting of a comparatively denser group of somas near the electrode tip and a sparse group of neurons located distant from the electrode. In short, the results described here support both the original studies by Stoney and the more recent study by Histed, painting a complex picture of spatial activation that is dependent on charge applied and time of observation during an extended pulse train[34,38].

Continuous electrical stimulation causes spatiotemporal somatic activation patterns in a frequency dependent manner

Our results also demonstrated that these two classes of activated somas, local and distant, have differing responses over time over the course of a 30 s pulse train that also vary based on stimulation frequency (Fig. 4b). In general, at lower frequencies activated somas both local and distant remained activated throughout the duration of the pulse train. At higher frequencies 90 Hz and above, distant somas activated at the beginning of the 30 s pulse train ceased to remain active by the end of the pulse train, with the Activation Time

progressively shorter as the frequency was increased. The temporal response based on frequency may in part explain the contradicting results between Histed and other historic studies. If measurements were only taken near the end of an extended pulse train, especially at high frequencies, only the dense activation of local soma would be observed[38]. Consistent with Histed's observation that the activation of distant soma were attributable to local activation of connected axons near the electrode, the temporal response of the neuropil near the electrode after somas were subtracted across frequencies paralleled the frequency dependent temporal responses of distant somas, suggesting that the somatic response is caused by changes in activation of the associated axons over the course of the pulse train[38].

The frequency dependent inactivation of axons local to the electrode over the course of an extended pulse train may provide insight on a potential mechanism of action for electrical stimulation for specific therapeutic uses[64,65]. For example, as DBS of the subthalamic nucleus (STN) to treat the tremor associated with Parkinson's Disease was originally based on the positive results of lesioning the same area, STN DBS was originally thought to generate the equivalent of a titratable/reversible lesion of STN. Following studies utilizing microwires for electrophysiological recordings - which are biased towards sampling action potentials initiated at the axon hillock where the axon meets as this is where the largest current deflection occurs – suggested that therapeutic DBS parameters in the 130 Hz range differentially suppress the activity of local STN somas while still activating local axons projecting to the targets from STN nuclei[66]. This led to the suggestion that DBS may be creating an information lesion of physiological signal passing through STN, as entrainment at 130 Hz would prevent physiological signal with temporal information content from being passed due to the stimulus rate and the absolute and relative refractory period of a neuron[67,68]. More recently antidromic activation of tracks of passage traveling near STN from motor cortex, known as the hyperdirect pathway, have received increasing attention as a potential mechanism to ameliorate pathological thalamocortical oscillations driving tremor in Parkinson's Disease[69-71]. The results in the present study demonstrate that stimulation at high frequencies associated with therapeutic DBS initially activates both local soma and local axons connected to distant somas, but over time the evoked activity in local axons projecting to distant somas decreases. These data suggest that to understand the post-synaptic response to stimulation - and ultimately the therapeutic mechanisms of action - one must account for differential activation of axons vs somas near the electrode, as well as changes in the local differential activation profile as a function frequency and time.

Frequency influences changes in degree of activation of different neuronal elements

The idea that different elements of the neuron may be activated or inactivated at different applied currents is not new[72,73]. It is often assumed, however, this differential evoked response local to the electrode is primarily a function of charge applied (current*pulsewidth) at frequencies at which pulse to pulse entrainment is feasible (130 Hz or less), given stimulation is within the Shannon/McCreery safety limits[58,59]. In this paradigm, changes in evoked network response as a function of frequency and time over the duration of pulse train are presumed to be post-synaptically mediated, for example as a function of vesicular depletion at the synapse leading to synaptic depression[74]. The data in the present study demonstrate that the responses of local axons versus somas differentially change over the course of an extended pulse train, and that frequencies over 50 Hz lead to initial activation but eventually the evoked activity of local axons over the course of the pulse train decreases. This may be very important for understanding the therapeutic mechanisms of action of electrical stimulation, especially in combination with drug administration acting on post-synaptic receptors, as well as lead to new stimulation paradigms leveraging knowledge of the response over time to preferentially stimulate local somas vs axons.

The mechanism by which increasing frequency may cause transient activation of axons local to the electrode followed by inactivation over the pulse train is presently not understood. Continuous stimulation could cause intermittent failure to propagate action potential through the axon at frequencies as low as 30 Hz, putatively mediated by extracellular accumulation of K^+ ions, depletion of ATP, and reduced inward Na^+ current[75]. Alternatively, Ranck et al have demonstrated that increasing intensities of cathodic stimulation may generate a distant virtual anode sufficient to hyperpolarize a stimulated fiber to the extent that any action potential initiated near the cathode is blocked from propagating by the virtual anode[35]. It is unclear whether higher frequencies could generate a similar effect due to a slower time constant for discharging the physiological capacitor at a biofouled electrode/electrolyte interface or at the lipid bilayer of the neural element. However, it is well understood that stimulation at very high frequencies (~10 kHz) can lead to block of neural activity in isolated fibers in the periphery. Moreover, McCreery, et al., has demonstrated that continuous stimulation for periods of

only seven hours can lead to Stimulation Induced Depression of Excitability (SIDNE)[76,77]. Other studies showed that continuous stimulation as short as 1 hr/day could lead to significantly different behavioral outcomes[78,79]. However, local activation and then subsequent decreased activation of local axons and their connected soma over the course of much shorter 30 second pulse trains suggest an underlying mechanism that has not been previously reported.

While inhibitory neurons are able to spike at higher rates than excitatory neurons, active cells in this study are mostly excitatory, indicating a persistence of activity with sustained stimulation and not higher spike rates (as observed in the plateau in fluorescence change in Fig. 5)[40,80]. In this fashion, the lack of excitation observed at high frequency stimulation may be due to increased inhibitory neuron activity (non-GCaMP expressing) near the stimulation site. In addition, various studies have demonstrated that electrical stimulation can cause diverse effects such as increases in hippocampal and thalamic volume, increases in blood vessel size and synaptic density, cortical dendrite growth, and changes in mRNA expression, some of which may influence short term local somatic and axonal response[81-94]. Future studies should be aimed at the difficult task of disentangling the complex network of dendrites, axons, and cell bodies of inhibitory and excitatory cells that may be present near the electrode in the brain[72]. Without complete understanding of how an exogenous electric field is interacting with neuronal and non-neuronal cells local to a chronically implanted electrode at the targeted point of intervention - and activating or inhibiting individual elements of these cells types – it is difficult to understand the mechanism by which targeted electrical stimulation may be creating desired therapeutic outcomes or undesirable side effects.

Calcium Activity under anesthesia

Under normal conditions, neuronal depolarization causes an influx of intracellular calcium through pathways such as voltage or neurotransmitter gated Ca^{2+} channels, which is measured by the GCaMP indicator[95]. The calcium influx then leads to a significant contribution from Ca^{2+} release through channels present in intracellular stores, mainly the endoplasmic reticulum[96]. Intracellular calcium can then induce local changes at the synaptic level and activate gene expression that are essential for synaptic plasticity[95]. Calcium activity has also been previously demonstrated during microelectrode insertion[97]. In order to prevent the mechanical strain related Ca activity influence stimulation evoked GCaMP activity, the tissue was allowed to rest 20 minutes after insertion prior to stimulation experiments, which was confirmed during the pre-stimulus period.

Active cells were identified as cells with intensity increased greater than 3 standard deviations of their pre-stimulation baseline fluctuation. While it is possible that the threshold selection might not have identified all active cells, GCaMP6s is very sensitive to neuronal activity even for single action potentials (>30% dF/F reported)[45]. Our criteria was robust for detection of low levels of activity even in the presence of small, unwanted signal changes due to motion or photomultiplier tube (PMT) dark current. Because the animal was under anesthesia, there was limited spontaneous activity as seen in pre-stimulation images in Figures 2 and 3. This likely helped detect stimulation-evoked activity in most GCaMP expressing neurons. In this study, calcium imaging was carried out at 50 μA, but it is worth nothing that in one animal, the impedance of the stimulated site was an order of magnitude lower than that listed by the manufacturer, suggesting insulation failure or other forms of shunting with the ground. In this animal, 100 μA stimulation current was necessary to drive GCaMP activity.

Further studies are necessary to better understand the cause of inhibition of calcium activity at higher frequencies. Examining the influence of downstream post-synaptic neuron activity will be an important step towards understanding the impact of stimulation frequency on the spatial distribution of activated neurons. It is possible that this frequency-dependent excitatory and inhibitory (or lack of excitation) pattern is the result of the interaction between the imposed changes in electric field and different neuronal processes in space. Lastly, the calcium impact on long-term changes in expressions of genes and synaptic properties further needs to be elucidated.

Additional considerations for chronic continuous electrical stimulation

In chronic neuromodulation or neuroprosthetic applications, additional complexities are entangled from tissue changes in both the neuronal and non-neuronal populations due to the implantation injury (glia,

neurovasculature, immune cells)[39,98-101], electrode material degradation[59,102-106], and plastic changes from long-term electrical stimulation[81-94,107]. For example, it is well understood that continuous stimulation at parameters above the safety limits (k>1.7~1.85) established by the Shannon curve can cause damage to tissue in the vicinity of the electrode, which is often attributed to driving toxic electrochemical reactions at the surface of the electrode, or driving local neural tissue to increase activity beyond physiological norms leading to 'excitotoxic' effects[58,59,81,107-109]. While this present study was carried out below the Shannon limit, the biological substrates of plasticity induced by clinically relevant stimulation parameters (below the Shannon Limit) over time are not well understood.

Limitations: In order to minimize the impact of SIDNE in this stimulation experiment and results, stimulation frequencies were evaluated in increasing frequencies instead of randomizing the frequency order. However, care was taken to allow baseline intensities to return to pre-stimulation baseline before another frequency was tested. Future studies should randomize one stimulation frequency to each implant location as well as evaluate the impact of the total number of stimulation pulses compared to stimulation frequency on driving SIDNE. A better understanding of these effects may further facilitate the application of continuous stimulation toward the growing field of neuromodulation therapies.

Conclusion

Despite the widespread use of electrical stimulation as a scientific tool and a modality to affect therapeutic outcomes, a lack in understanding of its effects on network-level neural activity has limited its applicability. While the present work is not a complete study on the large parameter space of electrical stimulation, we demonstrate that different stimulation parameters can dramatically alter the activation pattern at the cellular level in cortex. A deeper understanding of electrical stimulation parameters on neuronal activation (and non-neuronal activation) will be critical in utilizing electrical stimulation for targeted applications in basic science research as well as clinical therapeutics.

Methods

Surgery and electrode implantation
Transgenic mice C57BL/6J-Tg(Thy1 GCaMP6s)GP4.3Dkim/J (n=5, male, 22–28 g, Jackson Laboratories; Bar Harbor, ME) were used in this experiment. All animals were induced with an anesthetic mixture consisting of 75 mg/kg ketamine and 7 mg/kg xylazine administered intraperitoneally and updated with 40 mg/kg as needed. Craniotomies ~4 mm were made over each somatosensory cortex and electrodes were implanted at a 30º angle as previously described[39,46-50]. Electrical stimulation was conducted through a single-shank 16-channel Michigan style functional silicon probes with 703 μm^2 electrode sites (NeuroNexus Technologies, Ann Arbor, MI). All experimental protocols were approved by the University of Pittsburgh, Division of Laboratory Animal Resources and Institutional Animal Care and Use Committee in accordance with the standards for humane animal care as set by the Animal Welfare Act and the National Institutes of Health Guide for the Care and Use of Laboratory Animals.

Two-photon Imaging
A two-photon laser scanning microscope (Bruker, Madison, WI) and an OPO laser (Insight DS+; Spectra-Physics, Menlo Park, CA) tuned to a wavelength of 920 nm was used for this study. A16X 0.8 numerical aperture water immersion objective lens (Nikon Instruments, Melville, NY) was selected for its 3 mm working distance. Before imaging sessions, animals were injected with 0.1 ml of 1mg/ml SR101 for visualization of electrode contacts. Imaging plane was positioned 10 μm above the electrode site. In order to image neural dynamic during electrical stimulation, time series images were recorded at 30 Hz and 2x optical zoom. Imaging plane for time series were set right over the electrode contact, so that the stimulating contact is visible during imaging session.

Electrical stimulation
Stimulation protocols and imaging typically were performed 20 minutes after electrode implantation to allow time for displaced tissue to settle. A-M System 2100, single channel Isolated Pulse Stimulator (A-M Systems, Sequim, WA) or TDT IZ2 stimulator on an RZ5D system (Tucker-Davis Technologies, Alachua, FL) was used to apply current controlled cathodic leading biphasic symmetric (50 μs each phase) electrical microsimulation

at 10 Hz, 30 Hz, 50 Hz, 75 Hz, 90 Hz, 130 Hz and 250 Hz frequency and stimulating current of 50 μA. In one animal, 100 μA was required to evoke a visible response. Amplitude of stimulation was selected based on minimum current required to evoke activation during two photon live scanning. Charge/phase, charge density/phase and k values were calculated based on the Shannon's equation[58]. The *k* value used during stimulation was between -0.12 and 1.3, well within safety limits to avoid tissue damage. After collecting 2 min of resting state activity, electrical stimulation was imaged for 2 min at each frequency, which included 30 s of pre-stimulation baseline, 30s of stimulation and 60s of post-stimulation baseline. The two-photon microscope was synchronized to the stimulator via transistor-transistor logic and 30 s stimulation was carried out after a 30 s delay from the start of the T-series.

Data analysis

Identification of activated neurons

Time series images collected during experiments were converted to a single tiff image file using ImageJ (NIH). The tiff image was then analyzed using a custom MATLAB script (Mathwork, Natick, MA). To identify neurons, elliptical regions of interest (ROIs) were manually drawn around neurons, which were identified by their morphology as bright rings of fluorescence surrounding the soma (Fig 1b,d). Fluorescence intensity time-courses for each neuron were generated by averaging all pixels within a cell's ROI. Baseline fluorescence intensity (F_0) was calculated as the average signal during the 30-second pre-stimulation interval, and each time-course was then converted to a $\Delta F/F_0$. To identify activated neurons, each neuron's $\Delta F/F_0$ signal during stimulation was compared with their pre-stimulation $\Delta F/F_0$ signal. A fluorescence threshold of the mean pre-stimulation signal + three standard deviations (SD) was then established, such that neurons which showed $\Delta F/F_0$ changes that exceeded the threshold during stimulation were considered activated.

Neuropil Activation

Neuropil intensity was quantified by averaging the intensity level of a 10 μm by 25 μm regions that did not contain neuronal somas. For each frequency, the neuropil was measured in the following distances from the edge of the electrode; 10-20, 30-40, 50-60, 100-110, 150-160, and 245-255 μm. Similarly, representative neuronal somas were selected at 15 and 115 μm from the electrode. F/F_0 of GCaMP intensities were computed where F_0 was the average GCaMP intensity of the 30 s pre-stimulus period.

Temporal activation pattern

Somas were classified as onset-responsive if they were activated during the first 0-2 seconds of the 30 second pulse train but ceased activation before the final 2 seconds of the pulse train (28-30 s). Somas were classified as steady-state-responsive neurons if they were active during 28-30 s post-stimulation onset. Duration of activity was calculated for each neuron by considering all time-points during stimulation which exceeded the intensity threshold. To examine the temporal characteristics of activated neurons in local vs distant or dense vs sparse groups, a weighted response time was estimated for each neuron. The 'Activation Time' (τ) was calculated as the time at which the cumulative intensity reached 50% of the maximum cumulative ΔF/F signal change during the stimulation period (*t* between 0 to 30 s);

$$\int_{t=0}^{\tau} \frac{\Delta F(t)}{F} dt = 50\% * \int_{t=0}^{30} \frac{\Delta F(t)}{F} dt$$

where *dt* represents the frame period. This expression describes the time it takes to cover half of the response energy. For example, a soma that reaches peak intensity at 0 seconds into the pulse train and maintains the exact same ΔF/F for all 30 s would have an 'Activation Time' of 15 s. Similarly, a soma that maintains a peak ΔF/F from 0 s to 5 s, but then falls to 20% of peak ΔF/F from 5 s to 30 s would have an 'Activation Time' of 5 s.

Spatial activation pattern

The spatial relationship between stimulation frequency and activation pattern was determined by measuring the distance from the center of each active neuron to the nearest edge of the stimulating electrode site. The location of the center of the stimulating electrode site was visually identified from the same image series that was used to identify activated neurons, and was confirmed with a high-resolution image taken immediately before the trial. Activated neurons were separated into local and distant populations by establishing a threshold of the mean distance from the electrode site + 1SD. The cells which contained centers that were encompassed

by this distance threshold were considered local neurons, and those beyond this distance threshold were considered distant neurons.

Activation density

Density was examined as an independent measure by creating concentric circular bins, with an increasing radius of 20 μm drawn around the center of the electrode site. The number of fully encompassed, activated neurons within the area defined by each bin were counted from 0 to 30 s post stimulation onset, and then divided by the total area encompassed by that bin. Activated neurons were separated into dense or sparse populations, by establishing a threshold of mean density + 1 SD. To compare high and low-density activation patterns across stimulation frequencies, density thresholds were established for all stimulation frequencies, and the lowest mean density threshold was applied to all trials.

Statistical analysis

A one-way ANOVA, followed by post-hoc analysis with a Bonferroni correction was performed to assess significance between stimulation frequencies. Comparisons between groups (i.e. local vs distant, onset vs steady-state) were tested using a two-sample unequal variance T-test. All data in figures and text are reported as mean ± standard error.

Acknowledgements:
This work was supported by NIH NINDS R01NS094396, R01NS094404, R01NS062019, and R01NS089688. The authors would like to thank James R. Eles for technical and surgical assistance with the pilot study.

Author Contribution:
T.D.Y.K., A.L.V., and K.A.L. designed the experiment, and T.D.Y.K. carried out the experiment. N.J.M. and T.D.Y.K. planned the analysis. N.J.M. and R.I. carried out the analysis. All authors edited the manuscript.

Declaration of Interest:
The authors declare no competing interests.

References

1 Adrian, E. D. & Bronk, D. W. The discharge of impulses in motor nerve fibres: Part I. Impulses in single fibres of the phrenic nerve. *The Journal of physiology* **66**, 81 (1928).

2 Adrian, E. D. *The basis of sensation*. (Christophers; London, 22 Berners Steeet, W. 1, 1928).

3 Adrian, E. D. & Matthews, R. The action of light on the eye. *The Journal of Physiology* **65**, 273-298 (1928).

4 Sherrington, C. *The integrative action of the nervous system*. (CUP Archive, 1910).

5 Galvani, L. & Aldini, G. *Aloysii Galvani... De viribus electricitatis in motu musculari commentarius cum Ioannis Aldini Dissertatione et notis. Accesserunt Epistolæ ad animalis electricitatis theoriam pertinentes*. (Apud Societatem Typographicam, 1792).

6 Galvani, L. D viribus electricitatis in motu musculari: Commentarius. *Bologna: Tip. Istituto delle Scienze, 1791; 58 p.: 4 tavv. ft; in 4.; DCC. f. 70* (1791).

7 Du Bois-Reymond, E. H. *Untersuchungen über thierische elektricität: bd., 1. abth*. Vol. 2 (G. Reimer, 1884).

8 Fritsch, G. & Hitzig, E. Ueber die elektrische Erregbarkeit des Grosshirns. Archiv fur Anatomie und Physiologie und wissenschaftliche Medizin. **37**, 300–332. (1870).

9 Volta, A. XVII. On the electricity excited by the mere contact of conducting substances of different kinds. In a letter from Mr. Alexander Volta, FRS Professor of Natural Philosophy in the University of Pavia, to the Rt. Hon. Sir Joseph Banks, Bart. KBPR S. *Philosophical transactions of the Royal Society of London* **90**, 403-431 (1800).

10 Hodgkin, A. L. & Huxley, A. F. A quantitative description of membrane current and its application to conduction and excitation in nerve. *J Physiol* **117**, 500-544 (1952).

11 Eccles, J. C. The neurophysiological basis of mind: the principles of neurophysiology. (1953).

12 Penfield, W. & Boldrey, E. Somatic motor and sensory representation in the cerebral cortex of man as studied by electrical stimulation. *Brain* **60**, 389-443 (1937).

13 Spiegel, E. A., Wycis, H. T., Marks, M. & Lee, A. Stereotaxic apparatus for operations on the human brain. *Science* **106**, 349-350 (1947).

14 Delgado, J. M., Hamlin, H. & Chapman, W. P. Technique of intracranial electrode implacement for recording and stimulation and its possible therapeutic value in psychotic patients. *Confin Neurol* **12**, 315-319 (1952).

15 Djourno, A., Eyries, C. & Vallancien, B. DE LEXCITATION ELECTRIQUE DU NERF COCHLEAIRE CHEZ LHOMME, PAR INDUCTION A DISTANCE A LAIDE DUN MICRO-BOBINAGE INCLUS A DEMEURE. *Comptes Rendus des Séances de la Société de Biologie et de ses Filiales* **151**, 423-425 (1957).

16 House, L. R. Cochlear implant: the beginning. *Laryngoscope* **97**, 996-997 (1987).

17 House, W. F. Cochlear implants. *Ann Otol Rhinol Laryngol* **85 suppl 27**, 1-93 (1976).

18 Doyle Jr, J., Doyle, J., Turnbull, F., Abbey, J. & House, L. ELECTRICAL STIMULATION IN EIGHTH NERVE DEAFNESS. A PRELIMINARY REPORT. *Bulletin of the Los Angeles Neurological Society* **28**, 148 (1963).

19 Dobelle, W. H., Mladejovsky, M. G. & Girvin, J. P. Artifical vision for the blind: electrical stimulation of visual cortex offers hope for a functional prosthesis. *Science* **183**, 440-444 (1974).

20 Dobelle, W. & Mladejovsky, M. Phosphenes produced by electrical stimulation of human occipital cortex, and their application to the development of a prosthesis for the blind. *The Journal of physiology* **243**, 553-576 (1974).

21 Cushing, H. A note upon the faradic stimulation of the postcentral gyrus in conscious patients. *Brain* **32**, 44-53 (1909).

22 Flesher, S. N. *et al.* Intracortical microstimulation of human somatosensory cortex. *Science translational medicine* **8**, 361ra141-361ra141 (2016).

23 Sem-Jacobsen, C. Depth-electrographic observations related to Parkinson's disease. Recording and electrical stimulation in the area around the third ventricle. *Journal of neurosurgery* **24**, Suppl: 388-402 (1966).

24 Sem-Jacobsen, C. Depth electrographic stimulation and treatment of patients with Parkinson's disease including neurosurgical technique. *Acta Neurologica Scandinavica* **41**, 365-376 (1965).

25 Hassler, R., Riechert, T., Mundinger, F., Umbach, W. & Ganglberger, J. Physiological observations in stereotaxic operations in extrapyramidal motor disturbances. *Brain* **83**, 337-350 (1960).

26 Alberts, W. W. *et al.* Stereotaxic surgery for Parkinsonism: clinical results and stimulation thresholds. *Journal of neurosurgery* **23**, 174-183 (1965).

27 Richardson, D. E. & Akil, H. Pain reduction by electrical brain stimulation in man. Part 1: Acute administration in periaqueductal and periventricular sites. *J Neurosurg* **47**, 178-183, doi:10.3171/jns.1977.47.2.0178 (1977).

28 Richardson, D. E. & Akil, H. Pain reduction by electrical brain stimulation in man. Part 2: Chronic self-administration in the periventricular gray matter. *J Neurosurg* **47**, 184-194, doi:10.3171/jns.1977.47.2.0184 (1977).

29 Mayer, D. J. & Liebeskind, J. C. Pain reduction by focal electrical stimulation of the brain: an anatomical and behavioral analysis. *Brain research* **68**, 73-93 (1974).

30 Gol, A. Relief of pain by electrical stimulation of the septal area. *Journal of the neurological sciences* **5**, 115-120 (1967).

31 Robert, F. *et al.* Electrical stimulation of the anterior nucleus of thalamus for treatment of refractory epilepsy. *Epilepsia* **51**, 899-908, doi:doi:10.1111/j.1528-1167.2010.02536.x (2010).

32 Marcos, V. *et al.* Subacute Electrical Stimulation of the Hippocampus Blocks Intractable Temporal Lobe Seizures and Paroxysmal EEG Activities. *Epilepsia* **41**, 158-169, doi:doi:10.1111/j.1528-1157.2000.tb00135.x (2000).

33 LifeScienceAlley. LifeScience Alley Neuromodulation Sector Report (https://issuu.com/lifesciencealley/docs/neuromod-issuu, 2015).

34 Stoney Jr, S., Thompson, W. & Asanuma, H. Excitation of pyramidal tract cells by intracortical microstimulation: effective extent of stimulating current. *Journal of neurophysiology* **31**, 659-669 (1968).

35 Ranck, J. B. WHICH ELEMENTS ARE EXCITED IN ELECTRICAL STIMULATION OF MAMMALIAN CENTRAL NERVOUS SYSTEM: A REVIEW. *Brain Research* **98**, 417-440 (1975).

36 Tehovnik, E. J. Electrical stimulation of neural tissue to evoke behavioral responses. **65** (1996).

37 Rattay, F. THE BASIC MECHANISM FOR THE ELECTRICAL STIMULATION OF THE NERVOUS SYSTEM. *Neuroscience Vol. 89, No. 2, pp. 335-346, 1999* (1999).

38 Histed, M. H., Bonin, V. & Reid, R. C. Direct activation of sparse, distributed populations of cortical neurons by electrical microstimulation. *Neuron* **63**, 508-522, doi:10.1016/j.neuron.2009.07.016 (2009).

39 Michelson, N. J. *et al.* Multi-scale, multi-modal analysis uncovers complex relationship at the brain tissue-implant neural interface: New Emphasis on the Biological Interface. *Journal of Neural Engineering* **15** (2018).

40 Dana, H. *et al.* Thy1-GCaMP6 transgenic mice for neuronal population imaging in vivo. *PLoS One* **9**, e108697, doi:10.1371/journal.pone.0108697 (2014).

41 Smetters, D., Majewska, A. & Yuste, R. Detecting action potentials in neuronal populations with calcium imaging. *Methods* **18**, 215-221 (1999).

42 Kerr, J. N. & Denk, W. Imaging in vivo: watching the brain in action. *Nature Reviews Neuroscience* **9**, 195 (2008).

43 Sato, T. R., Gray, N. W., Mainen, Z. F. & Svoboda, K. The functional microarchitecture of the mouse barrel cortex. *PLoS biology* **5**, e189 (2007).

44 Greenberg, D. S., Houweling, A. R. & Kerr, J. N. D. Population imaging of ongoing neuronal activity in the visual cortex of awake rats. *Nature neuroscience* **11**, 749-751, doi:10.1038/nn.2140 (2008).

45 Chen, T. W. *et al.* Ultrasensitive fluorescent proteins for imaging neuronal activity. *Nature* **499**, 295-300, doi:10.1038/nature12354 (2013).

46 Wellman, S. M. & Kozai, T. D. Y. In vivo spatiotemporal dynamics of NG2 glia activity caused by neural electrode implantation. *Biomaterials* **164**, 121-133 (2018).

47 Eles, J. R. *et al.* Neuroadhesive L1 coating attenuates acute microglial attachment to neural electrodes as revealed by live two-photon microscopy. *Biomaterials* **113**, 279-292 (2017).

48 Kozai, T. D. Y., Eles, J. R., Vazquez, A. L. & Cui, X. T. Two-photon imaging of chronically implanted neural electrodes: Sealing methods and new insights. *Journal of Neuroscience Methods* **256**, 46-55, doi:http://dx.doi.org/10.1016/j.jneumeth.2015.10.007 (2016).

49 Kozai, T. D. Y., Jaquins-gerstl, A. S., Vazquez, A. L., Michael, A. C. & Cui, X. T. Dexamethasone retrodialysis attenuates microglial response to implanted probes in vivo. *Biomaterials* **87**, 157-169, doi:10.1016/j.biomaterials.2016.02.013 (2016).

50 Kozai, T. D., Vazquez, A. L., Weaver, C. L., Kim, S. G. & Cui, X. T. In vivo two-photon microscopy reveals immediate microglial reaction to implantation of microelectrode through extension of processes. *J Neural Eng* **9**, 066001, doi:10.1088/1741-2560/9/6/066001 (2012).

51 Kozai, T. D. Y. *et al.* Reduction of neurovascular damage resulting from microelectrode insertion into the cerebral cortex using in vivo two-photon mapping. *J Neural Eng* **7**, 046011, doi:S1741-2560(10)46092-9 [pii]
10.1088/1741-2560/7/4/046011 (2010).

52 Shepherd, R. K. & Javel, E. Electrical stimulation of the auditory nerve: II. Effect of stimulus waveshape on single fibre response properties. *Hearing research* **130**, 171-188 (1999).

53 Wu, Y., Levy, R., Ashby, P., Tasker, R. & Dostrovsky, J. Does stimulation of the GPi control dyskinesia by activating inhibitory axons? *Movement Disorders* **16**, 208-216 (2001).

54 De Balthasar, C. *et al.* Channel interactions with high-rate biphasic electrical stimulation in cochlear implant subjects. *Hearing research* **182**, 77-87 (2003).

55 Kim, S. *et al.* Behavioral assessment of sensitivity to intracortical microstimulation of primate somatosensory cortex. *Proceedings of the National Academy of Sciences* **112**, 15202-15207 (2015).

56 Kent, A. & Grill, W. Recording evoked potentials during deep brain stimulation: development and validation of instrumentation to suppress the stimulus artefact. *Journal of neural engineering* **9**, 036004 (2012).

57 Lilly, J. C., Hughes, J. R., Alvord, E. C., Jr. & Galkin, T. W. Brief, noninjurious electric waveform for stimulation of the brain. *Science* **121**, 468-469 (1955).

58 Shannon, R. V. A model of safe levels for electrical stimulation. *IEEE Trans Biomed Eng* **39**, 424-426, doi:10.1109/10.126616 (1992).

59 Cogan, S. F., Ludwig, K. A., Welle, C. G. & Takmakov, P. Tissue damage thresholds during therapeutic electrical stimulation. *J Neural Eng* **13**, 021001, doi:10.1088/1741-2560/13/2/021001 (2016).

60 Wei, X. F. & Grill, W. M. Analysis of high-perimeter planar electrodes for efficient neural stimulation. *Frontiers in neuroengineering* **2**, 15 (2009).

61 Robinson, D. & Fuchs, A. Eye movements evoked by stimulation of frontal eye fields. *Journal of Neurophysiology* **32**, 637-648 (1969).

62 Murasugi, C. M., Salzman, C. D. & Newsome, W. T. Microstimulation in visual area MT: effects of varying pulse amplitude and frequency. *Journal of Neuroscience* **13**, 1719-1729 (1993).

63 Tolias, A. S. *et al.* Mapping cortical activity elicited with electrical microstimulation using FMRI in the macaque. *Neuron* **48**, 901-911 (2005).

64 Agnesi, F., Muralidharan, A., Baker, K. B., Vitek, J. L. & Johnson, M. D. Fidelity of frequency and phase entrainment of circuit-level spike activity during DBS. *Journal of neurophysiology* **114**, 825-834 (2015).

65 Gildenberg, P. L. Evolution of neuromodulation. *Stereotactic and functional neurosurgery* **83**, 71-79 (2005).

66 McIntyre, C. C., Grill, W. M., Sherman, D. L. & Thakor, N. V. Cellular Effects of Deep Brain Stimulation : Model-Based Analysis of Activation and Inhibition Cellular Effects of Deep Brain Stimulation : Model-Based Analysis of Activation and Inhibition. *Journal of Neurophysiology* **91**, 1457-1469, doi:10.1152/jn.00989.2003 (2004).

67 Grill, W. M., Snyder, A. N. & Miocinovic, S. Deep brain stimulation creates an informational lesion of the stimulated nucleus. *Neuroreport* **15**, 1137-1140 (2004).

68 Agnesi, F., Connolly, A. T., Baker, K. B., Vitek, J. L. & Johnson, M. D. Deep brain stimulation imposes complex informational lesions. *PLoS One* **8**, e74462 (2013).

69 Li, S., Arbuthnott, G. W., Jutras, M. J., Goldberg, J. A. & Jaeger, D. Resonant antidromic cortical circuit activation as a consequence of high-frequency subthalamic deep-brain stimulation. *Journal of neurophysiology* **98**, 3525-3537 (2007).

70 McIntyre, C. C. & Hahn, P. J. Network perspectives on the mechanisms of deep brain stimulation. *Neurobiology of disease* **38**, 329-337 (2010).

71 Gradinaru, V., Mogri, M., Thompson, K. R., Henderson, J. M. & Deisseroth, K. Optical deconstruction of parkinsonian neural circuitry. *Science* **324**, 354-359 (2009).

72 Overstreet, C., Klein, J. & Tillery, S. H. Computational modeling of direct neuronal recruitment during intracortical microstimulation in somatosensory cortex. *Journal of neural engineering* **10**, 066016 (2013).

73 McIntyre, C. C. & Grill, W. M. Extracellular stimulation of central neurons: influence of stimulus waveform and frequency on neuronal output. *Journal of neurophysiology* **88**, 1592-1604 (2002).

74 Wang, Y. & Manis, P. B. Short-term synaptic depression and recovery at the mature mammalian endbulb of Held synapse in mice. *Journal of neurophysiology* **100**, 1255-1264 (2008).

75 Smith, D. Mechanisms of action potential propagation failure at sites of axon branching in the crayfish. *J. Physiol. (1980), 301, pp. 243-259* (1980).

76 McCreery, D. B., Agnew, W. F. & Bullara, L. A. The effects of prolonged intracortical microstimulation on the excitability of pyramidal tract neurons in the cat. *Ann Biomed Eng* **30**, 107-119 (2002).

77 McCreery, D. B., Yuen, T. G., Agnew, W. F. & Bullara, L. A. A characterization of the effects on neuronal excitability due to prolonged microstimulation with chronically implanted microelectrodes. *IEEE transactions on bio-medical engineering* **44**, 931-939, doi:10.1109/10.634645 (1997).

78 White, J. J. & Sillitoe, R. V. Genetic silencing of olivocerebellar synapses causes dystonia-like behaviour in mice. *Nature Communications* **8**, 14912 (2017).

79 Hao, S. *et al.* Forniceal deep brain stimulation rescues hippocampal memory in Rett syndrome mice. *Nature* **526**, 430 (2015).

80 Makino, H. *et al.* Transformation of Cortex-wide Emergent Properties during Motor Learning. *Neuron* **94**, 880-890.e888, doi:10.1016/j.neuron.2017.04.015 (2017).

81 Agnew, W. F., Yuen, T. G., Pudenz, R. H. & Bullara, L. A. Electrical stimulation of the brain. IV. Ultrastructural studies. *Surgical neurology* **4**, 438-448 (1975).

82 Pudenz, R. H., Bullara, L. A., Dru, D. & Talalla, A. Electrical stimulation of the brain. II. Effects on the blood-brain barrier. *Surgical neurology* **4**, 265-270 (1975).

83 Brownson, C., Little, P., Jarvis, J. C. & Salmons, S. Reciprocal changes in myosin isoform mRNAs of rabbit skeletal muscle in response to the initiation and cessation of chronic electrical stimulation. *Muscle & nerve* **15**, 694-700, doi:10.1002/mus.880150611 (1992).

84 Morris, B. J., Feasey, K. J., ten Bruggencate, G., Herz, A. & Hollt, V. Electrical stimulation in vivo increases the expression of proenkephalin mRNA and decreases the expression of prodynorphin mRNA in rat hippocampal granule cells. *Proceedings of the National Academy of Sciences of the United States of America* **85**, 3226-3230 (1988).

85 Xia, Y., Buja, L. M., Scarpulla, R. C. & McMillin, J. B. Electrical stimulation of neonatal cardiomyocytes results in the sequential activation of nuclear genes governing mitochondrial proliferation and differentiation. *Proceedings of the National Academy of Sciences of the United States of America* **94**, 11399-11404 (1997).

86 Xia, Y. *et al.* Electrical stimulation of neonatal cardiac myocytes activates the NFAT3 and GATA4 pathways and up-regulates the adenylosuccinate synthetase 1 gene. *The Journal of biological chemistry* **275**, 1855-1863 (2000).

87 Gall, C., Murray, K. & Isackson, P. J. Kainic acid-induced seizures stimulate increased expression of nerve growth factor mRNA in rat hippocampus. *Brain research. Molecular brain research* **9**, 113-123 (1991).

88 Hirano, A., Becker, N. H. & Zimmerman, H. M. The use of peroxidase as a tracer in studies of alterations in the blood-brain barrier. *Journal of the neurological sciences* **10**, 205-213 (1970).

89 Baudry, M., Oliver, M., Creager, R., Wieraszko, A. & Lynch, G. Increase in glutamate receptors following repetitive electrical stimulation in hippocampal slices. *Life sciences* **27**, 325-330 (1980).

90 Sankar, T. *et al.* Deep Brain Stimulation Influences Brain Structure in Alzheimer's Disease. *Brain stimulation* **8**, 645-654, doi:10.1016/j.brs.2014.11.020 (2015).
91 Sankar, T. *et al.* Structural brain changes following subthalamic nucleus deep brain stimulation in Parkinson's disease. *Mov Disord* **31**, 1423-1425, doi:10.1002/mds.26707 (2016).
92 Chakravarty, M. M. *et al.* Deep brain stimulation of the ventromedial prefrontal cortex causes reorganization of neuronal processes and vasculature. *NeuroImage* **125**, 422-427, doi:10.1016/j.neuroimage.2015.10.049 (2016).
93 Veerakumar, A. *et al.* Antidepressant-like effects of cortical deep brain stimulation coincide with pro-neuroplastic adaptations of serotonin systems. *Biol Psychiatry* **76**, 203-212, doi:10.1016/j.biopsych.2013.12.009 (2014).
94 Cooperrider, J. *et al.* Chronic deep cerebellar stimulation promotes long-term potentiation, microstructural plasticity, and reorganization of perilesional cortical representation in a rodent model. *The Journal of neuroscience : the official journal of the Society for Neuroscience* **34**, 9040-9050, doi:10.1523/JNEUROSCI.0953-14.2014 (2014).
95 Berridge, M. J. Neuronal calcium signaling. *Neuron* **21**, 13-26 (1998).
96 Sharp, A. H. *et al.* Differential immunohistochemical localization of inositol 1, 4, 5-trisphosphate-and ryanodine-sensitive Ca2+ release channels in rat brain. *Journal of Neuroscience* **13**, 3051-3063 (1993).
97 Eles, J. R., Kozai, T. D. Y., Vazquez, A. L. & Cui, X. T. In vivo imaging of neuronal calcium during electrode implantation: spatial and temporal mapping of damage and recovery. *Biomaterials* (2018).
98 Salatino, J. W., Ludwig, K. A., Kozai, T. D. Y. & Purcell, E. K. Glial responses to implanted electrodes in the brain. *Nature BME* (2017).
99 Wellman, S. M. & Kozai, T. D. Y. Understanding the Inflammatory Tissue Reaction to Brain Implants To Improve Neurochemical Sensing Performance. *ACS Chemical Neuroscience*, doi:10.1021/acschemneuro.7b00403 (2017).
100 Kozai, T. D. Y., Jaquins-Gerstl, A., Vazquez, A. L., Michael, A. C. & Cui, X. T. Brain Tissue Responses to Neural Implants Impact Signal Sensitivity and Intervention Strategies. *ACS Chemical Neuroscience* **6**, 48-67, doi:10.1021/cn500256e (2015).
101 Kolarcik, C. L. *et al.* Evaluation of poly(3,4-ethylenedioxythiophene)/carbon nanotube neural electrode coatings for stimulation in the dorsal root ganglion. *Journal of neural engineering* **12**, 016008, doi:10.1088/1741-2560/12/1/016008 (2015).
102 Wellman, S. M. *et al.* A Materials Roadmap to Functional Neural Interface Design. *Advanced Functional Materials* **28**, 201701269, doi:10.1002/adfm.201701269 (2018).
103 Wilks, S. J. *et al.* Non-clinical and Pre-clinical Testing to Demonstrate Safety of the Barostim Neo Electrode for Activation of Carotid Baroreceptors in Chronic Human Implants. *Frontiers in neuroscience* **11**, 438, doi:10.3389/fnins.2017.00438 (2017).
104 Alba, N. A., Du, Z. J., Catt, K. A., Kozai, T. D. Y. & Cui, X. T. In vivo electrochemical analysis of a PEDOT/MWCNT neural electrode coating. *Biosensors* **5**, 618-646, doi:10.3390/bios5040618 (2015).
105 Kozai, T. *et al.* in *Nanotechnology and Neuroscience: Nano-electronic, Photonic and Mechanical Neuronal Interfacing* (eds Massimo De Vittorio, Luigi Martiradonna, & John Assad) Ch. Chapter 4: Nanostructured Coatings for Improved Charge Delivery to Neurons, 71-134 (Springer New York, 2014).
106 Cogan, S. F. Neural Stimulation and Recording Electrodes. *Annual Review of Biomedical Engineering* **10**, 275-309, doi:doi:10.1146/annurev.bioeng.10.061807.160518 (2008).
107 Merrill, D. R., Bikson, M. & Jefferys, J. G. Electrical stimulation of excitable tissue: design of efficacious and safe protocols. *Journal of Neuroscience Methods* **141**, 171-198, doi:S0165-0270(04)00382-6 [pii]
10.1016/j.jneumeth.2004.10.020 (2005).
108 Yuen, T. G., Agnew, W. F., Bullara, L. A., Jacques, S. & McCreery, D. B. Histological evaluation of neural damage from electrical stimulation: considerations for the selection of parameters for clinical application. *Neurosurgery* **9**, 292-299 (1981).
109 Mortimer, J. T., Shealy, C. N. & Wheeler, C. Experimental nondestructive electrical stimulation of the brain and spinal cord. *Journal of Neurosurgery* **32**, 553-559, doi:10.3171/jns.1970.32.5.0553 (1970).